Spin injection at remanence into III-V spin light-emitting diodes using (Co/Pt) ferromagnetic injectors

J. Zarpellon,[1,2] H. Jaffrès,[1,*] J. Frougier,[1] C. Deranlot,[1] J. M. George,[1] D. H. Mosca,[2] A. Lemaître,[3] F. Freimuth,[4] Quang Ha Duong,[5] P. Renucci,[5] and X. Marie[5]

[1]*Unité Mixte de Physique CNRS–Thales and Université Paris-Sud, Campus de Polytechnique, 1, Avenue Augustin Fresnel, 91767, Palaiseau, Cedex France*

[2]*Laboratório de Nanoestruturas para Sensores, Universidade Federal do Paraná, Centro Politécnico, Caixa Postal 19091, 81531-990 Curitiba, Brazil*

[3]*Laboratoire de Photonique et de Nanostructures, route de Nozay, 91460 Marcoussis, France*

[4]*Peter Grünberg Institut and Institute for Advanced Simulation, Forschungszentrum Jülich and JARA, 52425 Jülich, Germany*

[5]*Université de Toulouse, INSA-CNRS-UPS, LPCNO, 135 Avenue de Rangueil, 31077 Toulouse, France*

(Received 9 August 2012; published 19 November 2012)

We have studied the perpendicular magnetic anisotropy of Co/Pt multilayers and the electron spin injection efficiency by optical spectroscopy from a [Co(0.6 nm)/Pt(1 nm)]$_4$/Fe(0.3 nm)/MgO perpendicular tunnel spin injector grown on AlGaAs/GaAs semiconductor light-emitting diodes. We observe a 2.5% circular polarization at low temperature close to the magnetic remanence when the 0.3 nm Fe film of the ferromagnetic injector is sufficiently thin to maintain the magnetization out of plane. The acquired squared magnetization cycle is explained by the remaining interlayer exchange coupling existing between Fe and the (Co/Pt) multilayer through Pt or possible perpendicular magnetic anisotropy at the MgO/Fe interface. The corresponding spin polarization of the current is then estimated as 7%, measured by photoluminescence techniques, after the necessary up-renormalization, taking into account the electron spin-flip rate in the quantum well. In contrast, no circular polarization is observed when the thin Fe layer is removed and despite the rather high magnetic polarizability of the $5d^9$ electronic open shell of Pt at the interface with MgO. This emphasizes the reduced size of tunneling branching of wave functions at the interface, of the order of the atomic plane unit.

DOI: 10.1103/PhysRevB.86.205314 PACS number(s): 73.21.Ac, 72.25.Dc, 78.60.Fi

I. INTRODUCTION

Spintronics is a science that promotes the use of the charge and spin of carriers to implement additional functionalities in electronic devices.[1,2] In the field of semiconductors, spintronics becomes an alternative solution to standard electronics technology, which it is known will reach physical limitations in the near future.[3] This explains the large amount of work on spintronics with hybrid metal/semiconductor heterostructures for the past ten years, once it was proposed to solve the problem of impedance mismatch[4] by the use of an interface resistance, typically a tunneling barrier.[5–7] Various experiments have been performed to detect by electrical (e.g., the electrical Hanle effect) or by optical means a spin-polarized current injected from a ferromagnetic reservoir into a III-V semiconductor through an Al_2O_3 barrier,[8–12] through MgO,[12–16] and through GaO,[17] or into Si through Al_2O_3 (Refs. 18–22) and SiO_2 (Refs. 23–25) as well as into Ge through MgO.[26–34]

Among the latest experiments, the transformation of a spin-polarized electron current into left- or right-handed circularly polarized light in a spin light-emitting diode (spin LED) integrating a III-V semiconductor heterostructure[8,11,13–17,19,23,34,35] is one of the most striking physical phenomena. The electric dipolar selection rules involved in a quantum well[36] (QW) embedded in a spin LED during electron-hole recombination require spin injection with an out-of-plane magnetization. In most experiments, where the magnetization is constrained to lie in plane due to the dipolar interactions, a perpendicular magnetization is reached by the application of a strong magnetic field, of the order of 1 T or more, along the quantization axis normal to the QW plane. Up to now, very few experiments have been performed on tailored ferromagnetic/semiconductor heterostructures in a remanent state characterized by a spontaneous out-of-plane magnetization. This property can be provided by $3d/4d$ or $3d/5d$ ordered alloys in the fcc $L1_0$ cubic phase presenting alternate planes of magnetic and nonmagnetic atoms, as in CoPt(001),[37,38] FePt(001),[39] and FePd(001) (Ref. 40) compounds, or in $3d/4d$ or $3d/5d$ superlattices as in the cases of Co/Pd (Refs. 41–44) or Co/Pt systems.[43,45–47] With spin LEDs integrating out-of-plane magnetic media, Sinsarp *et al.*[48] obtained 1.5% as a lower estimate of the helicity of the light emitted at remanence at room temperature with an FePt/MgO spin injector. Hovel *et al.*[15] have more recently demonstrated a spin injection efficiency of about 3% at remanence using mixed $3d/4f$ transition metal/rare earth (Fe/Tb) media. More recently, Höpfner *et al.* obtained 3% of emitted light helicity at remanence using an (Fe/Tb)/MgO tunnel barrier as perpendicular spin injector and using InGaAs quantum dots as the active layer. Experiments performed on Si devices using a (Co/Pt)/Al_2O_3 spin injector[19] show clear hysteretic cycles of 1.2% amplitude.

In this paper, we will present experiments on spin injection into an AlGaAs/GaAs spin LED from a [Co(0.6 nm)/Pt (1 nm)]$_4$/Fe(0.3 nm)/MgO perpendicular spin injector, i.e., using a (Co/Pt) multilayer structure as out-of-plane magnetization spin injector, analyzing the degree of light helicity emitted from a 10 nm GaAs QW in the near infrared close to 800 nm wavelength. We observe a significant 2.5% circular light polarization close to the magnetic remanent state. This

indicates a 7% effective current spin polarization injected in the *n*-type AlGaAs semiconducting spacer, taking into account the loss of the light circular polarization in the QW. In Sec. II, we present the sample characteristics and its structural and magnetic characterization. In Sec. III, we focus on the magnetic properties (selective magnetic moments, out-of-plane anisotropy, interlayer exchange coupling) of [Co(0.6 nm)/Pt(t nm)](111)-textured multilayers grown by sputtering onto a 20 nm Pt(111)-oriented buffer on SiO_2. Detailed *ab initio* calculations performed in the full-potential linearized augmented plane-wave (FP-LAPW) method are presented in Sec. IV to analyze the spin-polarized electronic properties of the $3d/5d$ Co/Pt multilayer giving rise to the high perpendicular magnetic anisotropy (PMA) observed. Finally the results of electrical spin injection in spin LEDs probed by electroluminescence are discussed in Sec. V, where the total thickness of the multilayers has been made thin enough to allow optical transmission in the near infrared.

II. SAMPLE PREPARATION AND CHARACTERIZATION

(Co/Pt) multilayers were grown by sputtering at room temperature at a base pressure of about 5×10^{-8} mbar on two different templates. First, a series of samples (A) dedicated to magnetization measurements was fabricated on a thermally oxidized Si(001) wafer on which is grown a 20-nm-thick (111)-oriented fcc Pt buffer as checked by x-ray diffraction techniques; the nominal structure of these samples is SiO_2//Pt(20 nm)/[Co (0.6 nm)/Pt(X nm)]$_5$/Au (10 nm), with X varying from 0.4 to 2.6 nm. Second, a series of samples (B) prepared for spin injection experiments and optical detection consists of a (Co/Pt) multilayer grown on a 2.6-nm-thick MgO tunnel barrier deposited onto an AlGaAs/GaAs *n-i-p* diode and surmounted by a very thin (0.4–0.6 nm) Pt buffer layer in order to promote a quasi-two-dimensional growth. It then consists of a spin tunnel injector of the form MgO(2.6 nm)/Pt(X_{Pt} nm)/[(Co(0.6 nm)/Pt(1.0 nm)]$_4$/Au, with $X_{Pt} = 0.4$ and 0.6 nm. Finally, a third sample (C) was grown, characterized by the same sequence as samples B except that a thin 0.3 nm Fe film (typically two atomic planes) grown at 350 °C is now inserted between the MgO barrier and a 0.6-nm-thick Pt interlayer spacer in order to restore a quasifull spin polarization at the interface. 10-nm- and 3-nm-thick capping layer of Au and Pt, respectively, were used to prevent oxidization in each case. Spin light-emitting diodes have the following structure sequence: (001) substrate, $p = 2 \times 10^{19}$ cm^{-3}/p-$Al_{0.08}Ga_{0.92}As$-Be, $p = 1.7 \times 10^{19}$ cm^{-3} (500 nm)/undoped $Al_{x_{Al}}Ga_{1-x_{Al}}As$ (50 nm)/undoped GaAs quantum well (10 nm)/undoped $Al_{x_{Al}}Ga_{1-x_{Al}}As$ (50 nm)/n-$Al_{x_{Al}}Ga_{1-x_{Al}}As$ (50 nm), $n = 1 \times 10^{16}$ cm^{-3}/Si with $x_{Al} = 0.08$ and 0.15 respectively for series B and sample C. The surface was passivated with arsenic in the molecular-beam epitaxy chamber and then transferred in air into a magnetron sputtering system to grow the (Co/Pt)/MgO spin injector. Details of the preparation can be found elsewhere in the same kind of samples with tunnel injector.[14]

We present in Fig. 1(a) a cross-sectional transmission electron microscope (TEM) image of the SiO_2//Pt (20 nm)/[Co (0.6 nm)/Pt (1.0 nm)]$_5$/Au (10 nm) sample (sample series A). The TEM image reveals the SiO_2 substrate with a 20-nm-thick Pt buffer layer and Co/Pt multilayer formed by five chemically well defined bilayers covered by a 10-nm-thick Au capping layer as shown by the electron intensity profile. Figure 1(b) obtained from a selected area of Fig. 1(a) lightens the Z contrast between Co (peak) and Pt (valley) intensities due to the difference of electronic densities of these two atomic species. This evidences a clear chemical modulation. Consequently, as the Pt thickness increases above 0.4 nm (not shown), a well-defined chemical modulation appears within the (Co/Pt) multilayer with a typical Co-Pt interdiffusion thickness limited to one (or two) atomic planes. This particular (Co/Pt) sample exhibits a strong perpendicular magnetic anisotropy

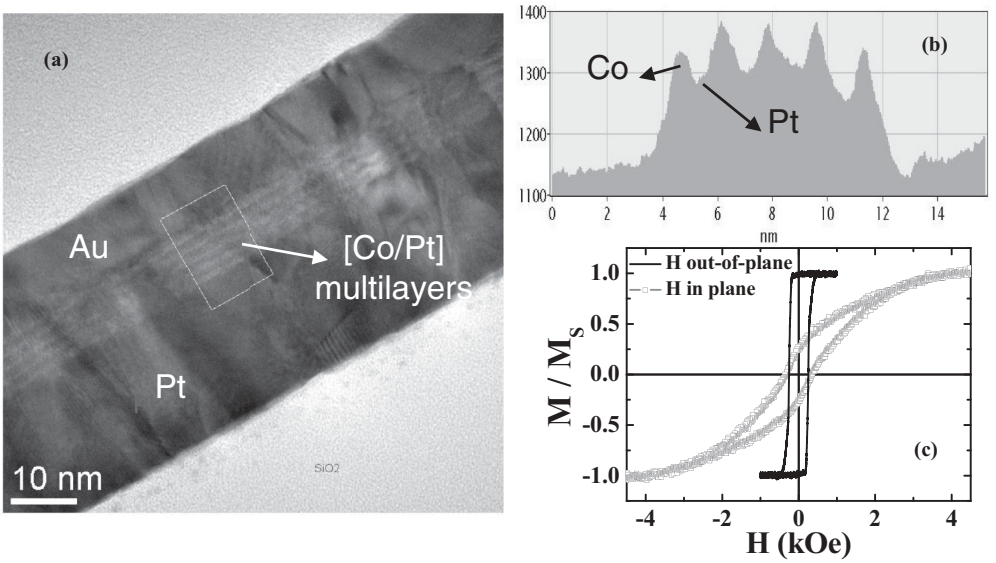

FIG. 1. (a) Cross-sectional TEM image of sample SiO_2//Pt (20 nm)/[Co (0.6 nm)/Pt (1.0 nm)]$_5$/Au (10 nm). (b) Electron intensity profile obtained from selected area shown in (a), revealing the stacking of alternate Co (peak) and Pt (valley) layers. (c) AGFM hysteresis loops for the same sample with magnetic field applied respectively in the out-of-plane and in-plane directions.

as indicated by the out-of-plane hysteresis cycle acquired at room temperature and displayed in Fig. 1(c). It is characterized by a coercive field of about 250 Oe for 1 nm Pt thickness. In contrast, the alternating gradient force magnetometer (AGFM) hysteresis loops measured with the magnetic field applied in the film plane [Fig. 1(c)] highlight a gradual rotation of the magnetization towards the in-plane direction up to a saturation field H_S close to 3 kOe. The latter quantity reveals the strength of the effective anisotropy field. These measurements indicate an in-plane magnetic hard axis and a strong PMA whose origin lies in the presence of a large interfacial anisotropy energy term K_S at each (Co/Pt) interface. After minimization of the overall free-energy density, the saturation field along the hard axis can be written $H_S \approx \frac{4K_S^{(Co/Pt)}}{t_{Co}M_S^{Co}} - 4\pi M_S^{Co}$,[49] where M_S^{Co} and t_{Co} are respectively the magnetization at saturation and the thickness of the Co layer in a single (Co/Pt) bilayer. This roughly gives $K_S^{(Co/Pt)} \simeq 0.5$ erg cm^{-2} per (Co/Pt) interface or $K_S^{(Co)} \simeq 1$ erg cm^{-2} per Co layer (or equivalently $K_S^{(Co)} \simeq 1$ mJ m^{-2} per Co layer).

Figure 2(a) displays the reflection high-energy electron diffraction (RHEED) pattern acquired on a 20-nm-thick Pt buffer grown on SiO_2. It clearly highlights a (111)-growth zone axis and a characteristic in-plane lattice parameter of 0.2275 nm corresponding to fcc Pt(111) of parameter $a = 0.391$ nm. The consecutive growth of a thin 0.6 nm Co layer [Fig. 2(b)] followed by a thin 1 nm Pt layer [Fig. 2(c)] does not alter the RHEED pattern, thus demonstrating that both Co and Pt layers adopt the in-plane parameter of the fcc (111) Pt buffer. In Fig. 2(d), we have reported the large-angle x-ray diffraction spectrum acquired on a SiO_2//Pt (20 nm)/[Co (0.6 nm)/Pt (1 nm)]$_3$/Pt (2 nm) multilayer. This exhibits the two corresponding (111) Pt and (111) Co peaks with the (111) Pt peak positioned at $2\theta = 39.6°$, corresponding to an interplane distance of $d = 0.227$ nm ($d \simeq a/\sqrt{3}$) from the formula $1/d = 2\sin(\theta)/\lambda_{k_\alpha^{Cu}}$. Note that the position of the Co peak is at a larger angle compared to the (111) Pt peak, which evidences a smaller interplane distance for Co of about 0.204 nm, close to one-half of the c parameter of bulk hcp Co ($c = 0.407$ nm). Moreover, complementary magnetic analysis (not presented) has shown that three monolayers of Pt (0.6 nm) were sufficient to promote a(111) texture favorable for obtaining a perpendicular magnetic anisotropy in (Co/Pt) multilayers. This explains our choice for the design of samples of series B and C grown on a thin MgO barrier onto LED structures and where the magnetic properties of the (Co/Pt) multilayers on the top are expected to keep their own intrinsic magnetic properties for PMA.

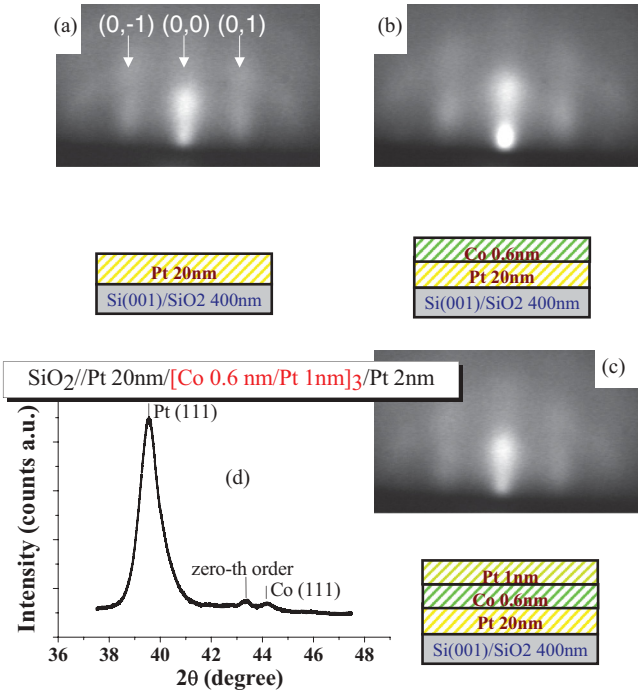

FIG. 2. (Color online) (a) Reflection high-energy electron diffraction (RHEED) pattern acquired on a 20-nm-thick Pt buffer grown on SiO_2, highlighting the (111)-growth zone axis. The in-plane atomic parameter corresponds to a (111) growth of fcc Pt. (b),(c) RHEED pattern acquired after the respective deposition of a 0.6 nm Co layer (b) and a 1 nm Pt layer (c), showing the same (111)-growth zone axis. Note that, in each case, the in-plane atomic parameter is the same as in (a). (d) Large-angle x-ray diffraction spectrum of SiO_2//Pt (20 nm)/[Co (0.6 nm)/Pt (1 nm)]$_3$/Pt (2 nm) displaying the two diffraction peaks corresponding, respectively, to Pt(111) and Co(111) (left and right peaks). The central peak matches the zero-order peak of the multilayer.

III. MAGNETIC PROPERTIES OF (111)-ORIENTED (Co/Pt) MULTILAYERS

We now address the effect of the Pt thickness on the magnetic properties for samples grown on a 20-nm-Pt buffer (series A), i.e., considering the SiO_2//Pt(20 nm)/[Co(0.6 nm)/Pt(X nm)]$_5$/Au (10 nm) samples, with X ranging from 0.4 to 2.6 nm. Figure 3 displays the different hysteresis loops acquired at room temperature for a magnetic field applied out of plane and corresponding to different Pt thicknesses (X lying between 0.2 and 1.4 nm). The squareness of the loop for $X > 0.4$ nm with an M_R/M_S ratio close to 1 (M_R is the remanent magnetization and M_S is the magnetization

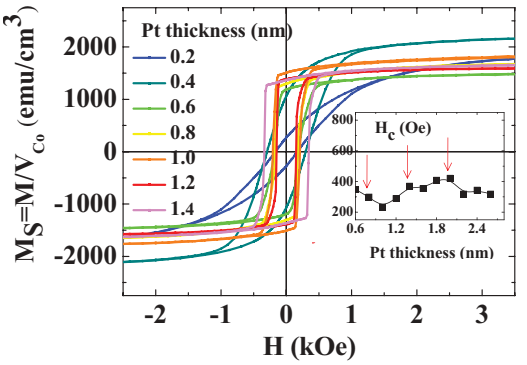

FIG. 3. (Color online) Sample series A: (a) Hysteresis loops measured at 300 K for an out-of-plane magnetic field for SiO_2//Pt (20 nm)/[Co(0.6nm)/Pt(X nm)]$_5$/Au(10 nm) with $X = 0.2$, 0.4, 0.6, and 0.8 nm. The $X = 1$, 1.2, 1.4, 1.6, 1.8, 2, and 2.6 nm samples (not shown) display square hysteresis cycles. Inset: Coercive field of (Co/Pt) multilayers vs Pt thickness displaying oscillations obtained on a different sample series.

at saturation) clearly demonstrates the presence of a strong PMA for the whole sample series when $X > 0.4$ nm. We observe the same behavior for $X > 1.4$ nm up to $X = 2.6$ nm (not shown). The characteristic hard-like shape of the magnetization hysteresis measured on the sample with $X = 0.2$ together with the reduced remanence $M_R/M_S \approx 0.65$ for $X = 0.4$ nm emphasize a loss of PMA properties for the thinnest Pt spacer. The same feature occurs for the smallest 0.2 nm Co thickness (not shown). This loss of PMA mainly results from the discontinuity of the coverage close to one Pt monolayer, at least for $X = 0.2$ nm, leading to interdiffusion and alloying between Co and Pt,[50] and finally to interfaces that are not chemically well defined at the length scale of one atomic plane. As in $CoPt_3$ in the $L1_2$ cubic phase considered as a model system, a local chemical disorder at interfaces has the effect of strongly reducing the PMA.[51] In the same spirit, Tyson *et al.*[52] measured by x-ray absorption the rise of PMA in the $L1_2$ $CoPt_3$ phase by the preferential formation of Co-Co (Co-Pt) atomic bonds in the in-plane (out-of-plane) direction, thus leading to same conclusion that a disorder, mixing the direction of (Co and Pt) chemical bonds, destroys the PMA. Another argument in favor of alloying and disorder in the thinnest Co or Pt layers is an anomalous increase of the magnetic moment at the (Co/Pt) interfaces due to the high magnetic polarizability of $5d^9$ Pt. We will come back to this point in Sec. IV dealing with *ab initio* calculations of the electronic properties of such Co/Pt multilayers.

Figure 4 displays the magnetization at saturation measured at room temperature (RT) on samples of series A vs the interlayer Pt thickness normalized by the effective Co volume in the corresponding multilayer. We observe in each sample an enhancement of the magnetization compared to the bulk hcp Co value of 1400 emu/cm^3 at RT. The average value for the thicker Pt spacer ($X > 0.6$ nm) roughly equals 1700 emu/cm^3, in rather close agreement with the data of Ref. 49 for Co

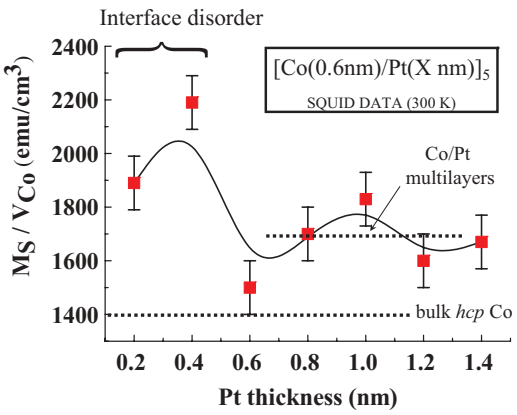

FIG. 4. (Color online) Sample series A: Magnetization at saturation (M_S) measured with a superconducting quantum interference device (SQUID) at 300 K of [Co(0.6 nm)/Pt(X nm)]$_5$ multilayers normalized to the Co volume vs the Pt thickness. Note the large enhancement of the magnetization for the thinnest Pt spacers due to Co-Pt interdiffusion and alloying. The average value of 1700 emu/cm^3 measured for the thicker Pt spacer exhibits an enhancement of the Co atomic magnetic moment together with a partial polarization of the Pt atoms at the (Co/Pt) interfaces (see the text).

(0.6 nm)/Pt(X nm) superlattices. An average enhancement of 300 emu/cm^3 per unit Co volume occurs, which results, first, in the magnetic polarization of the $5d^9$ configuration of Pt by hybridization with Co and, second, in a strong increase of the magnetic moment of Co itself. As an example, a reasonable total magnetic moment on Pt of the order of $0.5\mu_B$/atomic surface summed over all inner atomic planes[53–57] would give a magnetization at saturation of about 170 emu/cm^3 normalized to the effective Co volume. This should be complemented by an increase of the Co moment itself of about 130 emu/cm^3 ($+0.15\mu_B$/Co atom). The very large increase of the magnetic moment observed for the smallest Pt thickness ($X = 0.2$–0.4 nm), as high as 2200 emu/cm^3, may be assigned to the chemical disorder, Pt interdiffusion, and alloying at the Co/Pt interfaces as shown recently by Sipr *et al.*[58] and as calculated in the following section. The origin of the relative modest magnetic moment M_S measured on the $X = 0.6$ nm sample (1500 emu/cm^3) as well as the apparent oscillatory behavior of M_S around its average value (1700 emu/cm^3) for $X > 0.6$ nm, which seems to depart from the error bars, remains unclear.

Let us discuss the existence of a possible Ruderman-Kittel-Kayusa-Yosida interlayer exchange coupling[59] (IEC) in Co/Pt multilayers, as in the model by Bruno.[60] In the inset of Fig. 3, we display the oscillatory behavior of the coercive field H_C of the different samples vs the thickness of the Pt spacer, extracted from the hysteresis cycles acquired at 300 K, and as already observed in identical (Co/Pt) systems.[61–63] According to the conclusions of Ref. 61, such oscillations seem to indicate an intrinsic interlayer exchange coupling between adjacent Co layers mediated through Pt,[62,63] with two different oscillation periods of respectively 2.7 and 0.6 nm,[61] and as indicated by the arrows in the inset of Fig. 2 showing the 0.6 nm periodicity (the 2.7 nm periodicity cannot be seen). We will come back to the problem of IEC between Co and Fe in the [Co/Pt]/Fe system for the specific sample C for which significant circularly polarized light emitted from the corresponding spin LED in magnetic remanence appears, which may support this IEC scenario.

IV. MAGNETIC MOMENTS AND PERPENDICULAR MAGNETIC ANISOTROPY: FP-LAPW *ab initio* CALCULATIONS

Ab initio calculations of the selective magnetic moments and magnetic anisotropy in (Co/Pt) multilayers have been carried out within the density functional theory approach using the full-potential linearized augmented plane-wave formalism[64–67] implemented with the FLEUR code.[68,69] To describe electronic exchange and correlation, we employed the functional proposed by Perdew, Burke, and Ernzehof[70] within the generalized-gradient approximation. The spin-orbit coupling is treated from a fully relativistic point of view, which allows a self-consistent calculation of orbital moments and orbital anisotropy energy. The studied multilayers are composed of (111)-oriented Co(n)/Pt(m) infinite multilayers, where the indices n and m denote the numbers of atomic planes within the Co and Pt layers, respectively. The calculations have been carried out by considering the corresponding stacking sequences, i.e., AB-like hcp or ABC-like (111)-oriented fcc

TABLE I. Selective magnetic moments (μ_B/atom) and perpendicular magnetic anisotropy energy $\Delta\epsilon$ (μeV/atom) related to the different Co(n)Pt(m) multilayers. For thin Co layers (no more than three atomic planes), the in-plane hexagonal hcp structure has atomic parameter $a = 0.276$ nm, matching the (111)-oriented fcc Pt bulk lattice. This corresponds to an in-plane size expansion of the Co lattice of 10% compared to its bulk hcp value of 0.251 nm. The plane-to-plane interatomic distance was fixed to $d = 0.204$ nm in agreement with x-ray data. $CoPt_a$ (a indicating alloying) corresponds to a tetragonal structure of lattice parameters $a = 0.311$ nm and $b = 0.280$ nm with a Pt atom at each corner and a Co atom in the center. The first, second, third, and fourth lines correspond, respectively, to spin μ_S, orbital μ_L, and total μ_T magnetic moments [$\perp$ ($\parallel$) for out-of-plane (in-plane) magnetization]. The numbers (1),(2) in the first column index the Co and Pt atomic planes from the Co/Pt interface (1) to the inner plane of the bulk layers (2). M_S is the total magnetization at saturation. Magnetocrystalline Anisotropy (MCA) is the magnetic crystalline anisotropy, i.e., the difference of energy between in-plane and out-of-plane magnetic configurations.

Stacking sequence	Co(1)Pt(1) (*AB*)	Co(2)Pt(1) (*ABC*)	Co(2)Pt(2) (*AB*)	Co(3)Pt(1) (*ABC*)	Co(3)Pt(3) (*AB*)	Co(3)Pt(2) (*AB*)	$CoPt_a$ (*T*)
Co(1) $\mu_S^\perp$	1.925	1.880	1.915	1.875	1.905	1.925	1.975
$\mu_L^\perp$	0.085	0.110	0.105	0.110	0.115	0.115	0.105
$\mu_L^\parallel$	0.040	0.075	0.060	0.080	0.070	0.070	
$\mu_T^\perp$	2.010	1.990	2.020	1.985	2.020	2.040	2.080
Co(2) $\mu_S^\perp$				1.900	1.885	1.890	
$\mu_L^\perp$				0.105	0.120	0.120	
$\mu_L^\parallel$				0.105	0.095	0.100	
$\mu_T^\perp$				2.005	2.005	2.010	
Pt(1) $\mu_S^\perp$	0.370	0.27	0.330	0.30	0.310	0.310	0.385
$\mu_L^\perp$	0.060	0.05	0.110	0.05	0.040	0.050	0.105
$\mu_T^\perp$	0.430	0.32	0.440	0.35	0.350	0.360	0.490
Pt(2) $\mu_S^\perp$						0.225	
$\mu_L^\perp$						0.050	
$\mu_T^\perp$						0.275	
M_S (emu/cm$^3_{Co}$)	1670	1480	1680	1450	1470	1610	1760
MCA (μeV/Co atom)	790	490	1000	600	800	1100	x
MCA (mJ m^{-2}/Co layer)	1.9	2.4	4.9	2.7	3.6	4.9	x

stacking, giving the PMA and minimizing the total free energy with an in-plane lattice parameter of $a = 0.276$ nm, corresponding to the bulk (111) fcc Pt lattice. This corresponds to an in-plane size expansion of the Co lattice of $+10\%$ compared to its bulk hcp value of in-plane parameter $a =$ 0.251 nm. The plane-to-plane interatomic distance was fixed close to its bulk value of $d = 0.204$ nm as indicated by x-ray data, thus leading to an effective atomic volume of about 13.6 Å^3, in agreement with previous arguments given in Ref. 57 for the case of Co monolayers grown on a (111) Pt substrate. Second, in order to model the Co-Pt disorder or intermixing at each Co/Pt interface, we have calculated the magnetic moments induced by a (local) symmetry described by a $CoPt_a$ (a indicating alloying) tetragonal cell of lattice parameters $a = 0.311$ nm and $b = 0.280$ nm with a Pt atom at each corner and a Co atom at the center of the cell and the same atomic volume as the hexagonal structure described here. Such a (local) tetragonal structure mimics the maximal disorder between Co and Pt with the same interatomic distance and the same strain field as the (Co/Pt) multilayers described previously.

Results of the different calculations are gathered in Table I. Let us comment on the enhancement of the magnetic moments of [Co(0.6 nm)/Pt(X nm)]$_5$ multilayers reported in Fig. 4, corresponding to Co(3)/Pt(m) sequences where the magnetic moments on Co are seen to be enhanced compared to the hcp bulk ($1.74\mu_B$/atom) and where a significant magnetic moment appears on Pt. For the thicker Pt spacer (Fig. 4), the average magnetic moment, measured to be about 1700 emu/cm^3, is calculated to be equal to 1610 emu/cm^3 for Co(3)Pt(3), which is assumed to be representative of the Co(3)Pt(m) structures for $m \geqslant 3$ as the three Pt layers are assumed to contain the full magnetization of Pt of about $0.6\mu_B$/atom.[53–57] In this picture, the slight difference between the measured and calculated moments originates from Co-Pt alloying and interdiffusion, which can be schematically described by a thin $CoPt_a$ interdiffusion layer at each Co/Pt interface, leading to an enhancement of the magnetic moment from 1610 emu/cm^3 to about 1700 emu/cm^3, assuming that the value for the Co(3)Pt(3) structure can be roughly considered as an average between the Co(2)Pt(2) and $CoPt_a$ configurations. Correspondingly, the magnetic anisotropy for the [Co(0.6 nm)Pt(0.6 nm)]$_5$ multilayer [Co(3)Pt(3) structure], measured to be about 1 mJ m^{-2} per Co layer, is calculated to be 4.9 mJ m^{-2}/Co layer for Co(2)Pt(2) and Co(3)Pt(3) (Table I). Interface alloying and intermixing roughly decrease the PMA value to about one-half of 4.9 mJ m^{-2}/Co layer, that is, 2 mJ m^{-2}/Co layer, in rather close agreement with the experiments. This anisotropy value for (Co/Pt) is also in excellent agreement with the value of 690 μeV/Co atom obtained by local spin density approximation calculations for a Co monolayer.[57] However, the experimental Magnetic Anisotropy energy (MAE) for CoPt in the $L1_0$ phase appears to be stronger, of the order of 1–2 meV/Co atom,[37,38] in

agreement with calculations performed in the 1990s.[51,71,72] This larger MAE may be due to the higher number of Pt atoms neighboring each Co site. For the thinnest Pt spacer $X = 0.2$–0.4 nm [Pt and Pt(2)], the measured magnetic moment appears considerably larger than those calculated for Co(3)Pt(1), and Co(3)Pt(3) and their average value, expected to be close to that for Co(3)Pt(2). This indicates a strong enhancement of the magnetic moment due to Co-Pt interdiffusion and alloying, as calculated for the $CoPt_a$ tetragonal structure in Table I up to 1760 emu/cm^3. In parallel, the loss of the squareness of the out-of-plane magnetization cycles for the corresponding samples (thinnest Pt spacer) must be due to a lower PMA for the tetragonal structure compared to the hexagonal lattice, strongly reducing the magnetic moment at remanence.

Whereas the enhancement of the magnetic moment of Co (Table I) mainly originates from the in-plane size extension of the lattice parameter, the relatively small value of the Co average orbital moment μ_L (bulk value $0.14\mu_B$/atom) is explained by a larger strength of the out-of-plane $3d$-$5d$ Co-Pt bonds relative to the in-plane $3d$-$3d$ Co-Co bonds.[73] The result is a larger effective bandwidth for out-of-plane orbitals,[74] which is also responsible for the anisotropy of the Co orbital moment, with a difference $\mu_L^{\perp} - \mu_L^{\parallel}$ ($\mu_L^{\perp} > \mu_L^{\parallel}$) between the out-of-plane ($\perp$) and in-plane ($\parallel$) magnetization according to the argument of Stöhr.[74] Such anisotropy of μ_L, reported in Table I, appears naturally within the approach proposed by Bruno.[75] The PMA of transition metal alloys can be explained through a simple linear relationship between ΔE_{MCA} and $\mu_L^{\perp} - \mu_L^{\parallel}$ using a perturbative treatment at the second order for the spin-orbit interactions. This approach was refined later on by van der Laan[76] by including spin-mixing terms due to both majority- and minority-spin band contributions. It remains that a fair quantitative model requires consideration of orbital-dependent hybridization and selective charge and d-bandwidth anisotropy within a generalized *anisotropic ligand-field model* as was proposed in the early 2000s.[74]

V. INTERLAYER EXCHANGE COUPLING AND SPIN INJECTION PROBLEM

Polarization-resolved electroluminescence (EL) measurements performed on samples of series B and C allows us to probe the spin injection efficiency in the AlGaAs region from the $[Co/Pt]_n(Fe)/MgO$ perpendicular injector. The spin LEDs were placed in a cryostat into a Helmoltz split magnetic coil, providing a maximum magnetic field B of 8 kOe normal to the sample plane. The EL signal was detected in the Faraday geometry at a temperature of 20 K. The EL circular polarization $\mathcal{P}_C$ was analyzed through a $\lambda/4$ wave plate and a linear analyzer; it is defined as $\mathcal{P}_C = (I^{\sigma^+} - I^{\sigma^-})/(I^{\sigma^+} + I^{\sigma^-})$ where I^{σ^+} and I^{σ^-} are the intensities of the right- and left-circularly-polarized components of the luminescence, respectively. Figure 5 displays the results for sample B with $X_{\mathrm{Pt}} = 0.6$ nm under a saturation magnetic field of 5 kOe applied along the out-of-plane direction and under a bias of 2.5 V. It does not exhibit any measurable spin-polarized light emission around the peak emission located at around 806.5 nm [Fig. 5(a) and upper inset], whatever the level of the bias applied [lower inset of Fig. 5(a)]. We have

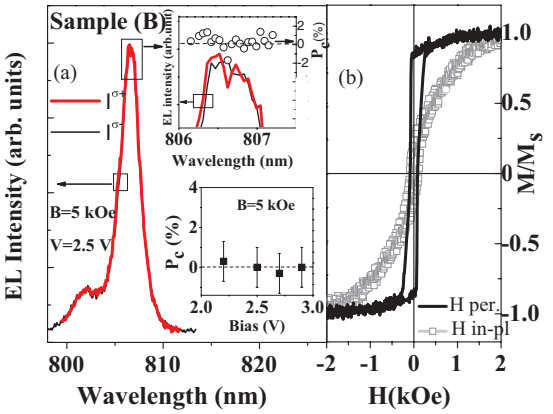

FIG. 5. (Color online) Sample series B series: $T = 20$ K. (a) Polarization-resolved electroluminescence (EL) spectra for $V = 2.5$ V under a saturating magnetic field of 5 kOe for sample B with $X_{\mathrm{Pt}} = 0.6$ nm. Respective intensities I^{σ^+} and I^{σ^-} of the right- (red thick line) and left-circularly-polarized (black thick line) EL components vs the emission wavelength. Upper inset: zoom around 806.5 nm; right axis, EL circular polarization (open circles). Lower inset: EL circular polarization measured at the peak emission vs the applied bias. (b) Out-of-plane (solid line) and in-plane (open squares) magnetization cycles.

also performed polarization-resolved EL measurements (not shown) on the sample B with $X_{\mathrm{Pt}} = 0.4$ nm in the same experimental conditions, and the optical circular polarization remains very low ($\leqslant 1\%$).

In sample C with $X_{\mathrm{Pt}} = 0.6$ nm, a thin 0.3 nm Fe layer has been inserted at the interface with MgO. For this sample, the quantum-well EL circularly polarized components I^{σ^+} and I^{σ^-} emitted at a wavelength of 800 nm are displayed in Fig. 6(a) (and the corresponding upper inset) under a saturation field of 0.45 kOe. In contrast to sample series A and B, one observes a clear nonzero circular polarization of the luminescence. The EL circular polarization is maximal, that is, $P_c = (3.0 \pm 0.7)\%$ for an applied bias of 2.4 eV [lower inset in Fig. 6(a)]. Figure 7 displays a $(2.5 \pm 0.7)\%$ EL polarization under the same level of bias at remanence, that is, without applied magnetic field. The spurious contribution due to magnetic circular dichroism (MCD) of the ferromagnetic layers, smaller than 0.3% in the present case, has been evaluated by measuring the EL polarization using an independent technique: polarization-resolved cw photoluminescence (PL) under linearly polarized light (see, for example, Refs. 15, 77, and 78) and a longitudinal magnetic field varying between -1 and $+1$ kOe. In such experiments, the quantum well embedded in the mesa structure is excited by a He-Ne laser ($\lambda = 632$ nm, corresponding to a photon energy of 1.96 eV, that is, above the AlGaAs gap). Owing to the linear polarization, the rates of electrons photogenerated with spins up and down are equal, as for the holes. This then normally leads to PL emission of unpolarized light from electron-hole recombination within the QW. The PL circular polarization measured remains from MCD related to the optical absorption coefficient of the magnetic multilayer itself. In PL experiments, the contribution from excitation and emission is twice as high compared to spin LED EL operations where the injection is made electrically. We show in Fig. 6 that the MCD contribution is negligible

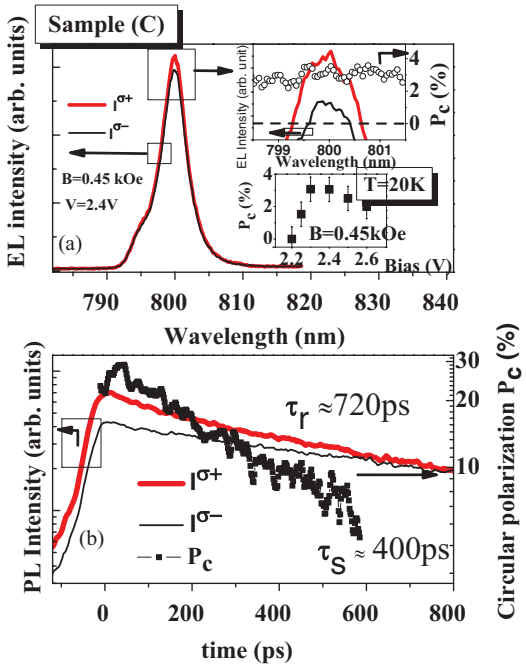

FIG. 6. (Color online) Sample C: $T = 20$ K. (a) Polarization-resolved electroluminescence (EL) spectra for $V = 2.4$ V under a magnetic field of 0.5 kOe for sample C with $X_{Pt} = 0.6$ nm and $t_{Fe} = 0.3$ nm. Respective intensities $I^{\sigma+}$ and $I^{\sigma-}$ of the right- (red thick line) and left-circularly-polarized (black thick line) EL components vs the emission wavelength. Upper inset: zoom around 800 nm; right axis, EL circular polarization (open circles). Lower inset: EL circular polarization measured at the peak emission *vs.* the applied bias. (b) Time- and polarization-resolved photoluminescence performed; left axis, $I^{\sigma+}$ (red thick line) and $I^{\sigma-}$ (black thin line) photoluminescence (PL) components vs time; right axis, corresponding PL circular polarization (open circles).

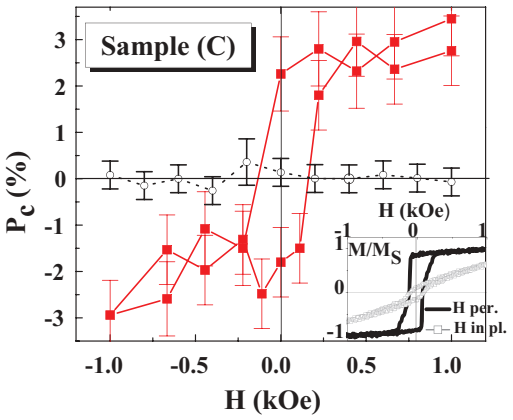

FIG. 7. (Color online) Sample C: $T = 20$ K. Full squares: EL circular polarization vs the applied magnetic field H for sample C with $X_{Pt} = 0.6$ nm and $t_{Fe} = 0.3$ nm ($V = 2.4$ V). Open circles: Photoluminescence circular polarization under excitation with a linearly polarized He-Ne laser ($E_{exc} = 1.96$ eV, excitation power $P = 300$ μW. Inset: Out-of-plane (solid line) and in-plane (open circles) magnetization cycles. The characteristic coercive field of about 280 Oe demonstrates the out-of-plane overall magnetization in the (Co/Pt)-Fe system.

(<0.3% in absolute value) compared to the EL circular polarization measured (2.5%–3.5%).

In order to extract the real electron spin polarization injected in the semiconductor QW, this value of 2.5% at remanence has to be up-renormalized by a typical factor of $(1 + \tau_r/\tau_{sf})$ (where τ_r is the recombination time, and τ_{sf} is the spin lifetime), in order to take into account the electron spin-relaxation time in the quantum well during electron-hole recombination.[14] In order to estimate τ_r and τ_{sf}, we have performed complementary time- and polarization-resolved photoluminescence experiments at 20 K under pulsed laser excitation (pulse width of about 1.5 ps from a mode-locked Ti:sapphire laser) at $E_{exc} = 1.670$ eV using a Si photocathode streak camera with an overall time resolution of about 8 ps. From the decays of the PL total intensity and the PL circular polarization as a function of time (Fig. 5), one can estimate $\tau_r \approx 735 \pm 30$ ps and $\tau_{sf} \approx 410 \pm 30$ ps. This leads to a factor $1 + \tau_r/\tau_{sf}$ close to 2.8, and a corresponding up-renormalization of the spin polarization of the electrons injected to about 7% at 20 K. Figure 7 describes the hysteresis cycle of the EL circular polarization (full squares) acquired at 20 K on sample C, matching quite well with the magnetization cycle of the whole magnetic injector (inset of Fig. 6). This clearly demonstrates an out-of-plane magnetization for the whole (Co/Pt)-Fe system together with an electrical spin injection from the thin Fe layer, at least at low temperature, by tunneling into AlGaAs. Such a small Fe thickness (about two atomic planes in the bcc phase) has been chosen to maintain the overall magnetization out of plane. In the limit of a strong ferromagnetic coupling between the (Co/Pt) multilayers and the Fe film, e.g., mediated by interlayer exchange coupling, the condition for out-of-plane magnetization is

$$\tfrac{1}{2} H_S M_S^{Co} \times N t_{Co} - 2\pi M_S^{Fe} \times t_{Fe} > 0, \qquad (1)$$

where H_S stands for the saturation field (or effective anisotropy field) in the film plane of the (Co/Pt) multilayer system, $N t_{Co}$ the effective thickness of Co, M_S^{Fe} the magnetization at saturation of Fe, and t_{Fe} the thickness of the Fe layer. This gives $t_{Fe} \leqslant 0.3$ nm, which strongly restricts the choice in the Fe thickness. Above this value, the overall magnetization should rotate in the plane of the films in the absence of any surface anisotropy at the Fe/Pt and Fe/MgO interfaces. However, at this stage, one cannot totally discard the idea that the corresponding perpendicular magnetic anisotropy arises, in part, from the contribution of an out-of-plane pure interfacial anisotropy between epitaxial MgO and Fe layers as argued by Yang *et al.* in a recent paper.[79]

Nevertheless, the relatively low value (7%) of the EL circular polarization measured compared to the spin polarization of Fe (about 40%) can be understood as coming from a certain discontinuity of the Fe layer on MgO owing to nonperfect epitaxial growth, leading to paramagnetic islands. This is supported by the decrease of the polarized EL signal which disappears over 70 K (not shown). Our experiments performed on series B clearly indicate a loss of the spin polarization of carriers injected from the Pt spacer, leading to a vanishing spin injection for $X_{Pt} = 0.6$ nm and 0.4 nm (two atomic planes). This results from the reduced extent of the tunneling branching of the corresponding wave function at barrier/metal interfaces with a characteristic length hardly exceeding one or

two atomic planes inside the metallic electrode.[80,81] Finally, our experiment performed on sample C seems to demonstrate a (ferromagnetic) interlayer exchange coupling between the Co/Pt multilayer and the thin Fe layer mediated through the 0.6-nm-thick Pt, as evidenced in a recently in the case of Pd/NiFe multilayers.[82]

VI. CONCLUSIONS

To conclude, we have performed a detailed study of (Co/Pt) multilayer systems grown by sputtering that exhibit an out-of-plane magnetization, focused on spin injection experiments in remanence in spin LED devices. The constraint of initiating the growth of (Co/Pt) multilayers on MgO barriers with Pt layers of thickness larger than $X_{\mathrm{Pt}} \geqslant 0.4$ nm leads to vanishing spin injection due to reduced magnetization at the Pt/MgO interfaces, the tunneling branching process operating at distances no more than two atomic planes from the interface. The insertion of a 0.3 nm Fe layer at the direct interface with MgO, sufficiently thin to maintain out-of-plane magnetization, allowsrestoration of a partial spin injection efficiency (an electroluminescence circular polarization of 2.5% is measured, corresponding to a spin polarization of the injected electrons of about 7% at low temperature and in the absence of any applied magnetic field). Complementary studies are currently being carried out to search for a possible PMA in MgO/CoFeB/Ta systems.

ACKNOWLEDGMENTS

We gratefully acknowledge T. Amand, F. Petroff, and A. Rogalev for fruitful discussions as well as D. Lagarde for her very efficient help in the estimation of the magnetic circular dichroism of the magnetic injector performed with polarization-resolved photoluminescence measurements. One of us (H.J.) would like to thank S. Blügel (Peter Grünberg Institut and Institute for Advanced Simulation, Forschungszentrum Jülich and JARA, Jülich, Germany) for his kind hospitality during H. J.'s stay at Jülich. This work was supported by the French Grant No. ANR-2010-BLAN-1014-1-INSPIRE and CAPES (Coordenãcao de Aperfeiçoamento de Pessoal de Nível Superior) in the CAPES-COFECUB Project No. 560/07.

*Present address: Peter Grünberg Institut and Institute for Advanced Simulation, Forschungszentrum Jülich and JARA, 52425 Jülich, Germany.

[1] C. Chappert, A. Fert, and F. Nguyen van Dau, Nat. Mater. **6**, 813 (2007).
[2] S. A. Wolf, D. D. Awschalom, R. A. Buhrman, J. M. Daughton, S. von Molnar, M. L. Roukes, A. Y. Chtchelkanova, and D. M. Treger, Science **294**, 1488 (2001).
[3] I. Zutic, J. Fabian, and S. Das Sarma, Rev. Mod. Phys. **76**, 323 (2004).
[4] G. Schmidt, D. Ferrand, L. W. Molenkamp, A. T. Filip, and B. J. van Wees, Phys. Rev. B **62**, 4790 (2000).
[5] E. I. Rashba, Phys. Rev. B **62**, R16267 (2000).
[6] A. Fert and H. Jaffrès, Phys. Rev. B **64**, 184420 (2001).
[7] A. Fert, J.-M. George, H. Jaffrès, and R. Mattana, IEEE Trans. Electron Devices **54**, 921 (2007).
[8] L. Lombez, P. Renucci, P. F. Braun, H. Carrère, X. Marie, T. Amand, B. Urbaszek, J. L. Gauffier, P. Gallo, T. Camps, A. Arnoult, C. Fontaine, C. Deranlot, R. Mattana, H. Jaffrès, J.-M. George, and P. H. Binh, Appl. Phys. Lett. **90**, 081111 (2007).
[9] M. Tran, H. Jaffrès, C. Deranlot, J.-M. George, A. Fert, A. Miard, and A. Lemaitre, Phys. Rev. Lett. **102**, 036601 (2009).
[10] S. P. Dash, S. Sharma, J. C. LeBreton, J. Peiro, H. Jaffrès, J.-M. George, A. Lemaître, and R. Jansen, Phys. Rev. B **84**, 054410 (2011).
[11] O. M. J. van't Erve, G. Kioseoglou, A. T. Hanbicki, C. H. Li, B. T. Jonker, R. Mallory, M. Yasar, and A. Petrou, Appl. Phys. Lett. **84**, 4334 (2004).
[12] P. Renucci, V. G. Truong, H. Jaffrès, L. Lombez, P. H. Binh, T. Amand, J.-M. George, and X. Marie, Phys. Rev. B **82**, 195317 (2010).
[13] X. Jiang, R. Wang, R. M. Shelby, R. M. Macfarlane, S. R. Bank, J. S. Harris, and S. S. P. Parkin, Phys. Rev. Lett. **94**, 056601 (2005).
[14] Y. Lu, V. G. Truong, P. Renucci, M. Tran, H. Jaffrès, C. Deranlot, J.-M. George, A. Lemaître, Y. Zheng, D. Demaille, P.-H. Binh, T. Amand, and X. Marie, Appl. Phys. Lett. **93**, 152102 (2008).
[15] S. Hovel, N. C. Gerhardt, M. R. Hofmann, F.-Y. Lo, A. Ludwig, D. Reuter, A. D. Wieck, E. Schuster, H. Wende, W. Keune, O. Petracic, and K. Westerholt, Appl. Phys. Lett. **93**, 021117 (2008).
[16] V. G. Truong, P.-H. Binh, P. Renucci, M. Tran, Y. Lu, H. Jaffrès, J.-M. George, C. Deranlot, A. Lemaitre, T. Amand, and X. Marie, Appl. Phys. Lett. **94**, 141109 (2009).
[17] H. Saito, J. C. Lebreton, V. Zayets, Y. Mireno, S. Yuasa, and K. Ando, Appl. Phys. Lett. **96**, 012501 (2010).
[18] O. M. J. van't Erve, A. T. Hanbicki, M. Holub, C. H. Li, C. Awo-Affouda, P. E. Thompson, and B. T. Jonker, Appl. Phys. Lett. **91**, 212109 (2007).
[19] L. Grenet, M. Jamet, P. Noe1, V. Calvo, J.-M. Hartmann, L. E. Nistor, B. Rodmacq, S. Auffret, P. Warin, and Y. Samson, Appl. Phys. Lett. **94**, 032502 (2009).
[20] S. P. Dash, S. Sharma, R. S. Patel, M. P. de Jong, and R. Jansen, Nature (London) **462**, 491 (2009).
[21] R. Jansen, B. C. Min, S. P. Dash, S. Sharma, G. Kioseoglou, A. T. Hanbicki, O. M. J. van't Erve, P. E. Thompson, and B. T. Jonker, Phys. Rev. B **82**, 241305 (2010).
[22] R. Jansen, Nat. Mater. **11**, 400 (2012).
[23] B. T. Jonker, G. Kioseoglou, A. T. Hanbicki, C. H. Li, and P. E. Thompson, Nat. Phys. **3**, 542 (2007).
[24] C. H. Li, G. Kioseoglou, O. M. J. van't Erve, P. E. Thompson, and B. T. Jonker, Appl. Phys. Lett. **95**, 172102 (2009).
[25] C. H. Li, O. M. J. van't Erve, and B. T. Jonker, Nat. Commun. **2**, 245 (2011).
[26] H. Saito, S. Watanabe, Y. Mineno, S. Sharma, R. Jansen, S. Yuasa, and K. Ando, Solid State Commun. **151**, 1159 (2011).
[27] S. Iba, H. Saito, A. Spiesser, S. Watanabe, R. Jansen, S. Yuasa, and K. Ando, Appl. Phys. Express **5**, 023003 (2012).
[28] S. Iba, H. Saito, A. Spiesser, S. Watanabe, R. Jansen, S. Yuasa, and K. Ando, Appl. Phys. Express **5**, 053004 (2012).
[29] A. Jain, L. Louahadj, J. Peiro, J. C. Le Breton, C. Vergnaud, A. Barski, C. Beigné, L. Notin, A. Marty, V. Baltz, S. Auffret, E. Augendre, H. Jaffrès, J.-M. George, and M. Jamet, Appl. Phys. Lett. **99**, 162102 (2011).

[30]A. Jain, C. Vergnaud, J. Peiro, J. C. Le Breton, E. Prestat, L. Louahadj, C. Portemont, C. Ducruet, V. Baltz, A. Marty, A. Barski, P. Bayle-Guillemaud, L. Vila, J.-P. Attané, E. Augendre, H. Jaffrès, J.-M. George, and M. Jamet, Appl. Phys. Lett. **101**, 022402 (2012).
[31]A. Jain, J.-C. Rojas-Sanchez, M. Cubukcu, J. Peiro, J. C. Le Breton, E. Prestat, C. Vergnaud, L. Louahadj, C. Portemont, C. Ducruet, V. Baltz, A. Barski, P. Bayle-Guillemaud, L. Vila, J.-P. Attané, E. Augendre, G. Desfonds, S. Gambarelli, H. Jaffrès, J.-M. George, and M. Jamet, Phys. Rev. Lett. **109**, 106603 (2012).
[32]K. R. Jeon, B. C. Min, Y. H. Jo, H. S. Lee, I. J. Shin, C. Y. Park, S. Y. Park, and S. C. Shin, Phys. Rev. B **84**, 165315 (2011).
[33]T. Hanbicki, S. F. Cheng, R. Goswami, O. M. J. van't Erve, and B. T. Jonker, Solid State Commun. **152**, 244 (2012).
[34]H. Hopfner, C. Fritsche, A. Ludwig, A. Ludwig, F. Stromberg, H. Wende, W. Keune, D. Reuter, A. D. Wieck, N. C. Gerhardt, and M. R. Hofmann, Appl. Phys. Lett. **101**, 112402 (2012).
[35]R. Fiederling, M. Keim, G. Reuscher, W. Ossau, G. Schmidt, A. Waag, and L. W. Molenkamp, Nature (London) **402**, 787 (1999).
[36]F. Meier and B. P. Zakharchenya, *Optical Orientation* (North-Holland, New York, 1984).
[37]P. Eurin and J. Pauleve, IEEE Trans. Magn. **5**, 216 (1969).
[38]W. Grange, I. Galanakis, M. Alouani, M. Maret, J.-P. Kappler, and A. Rogalev, Phys. Rev. B **62**, 1157 (2000).
[39]A. Cebollada, D. Weller, J. Sticht, G. R. Harp, R. F. C. Farrow, R. F. Marks, R. Savoy, and J. C. Scott, Phys. Rev. B **50**, 3419 (1994), and references therein.
[40]V. Gehanno, A. Marty, B. Gilles, and Y. Samson, Phys. Rev. B **55**, 12552 (1997).
[41]U. Gradmann and J. Muller, Phys. Status Solidi **27**, 313 (1968).
[42]P. F. Carcia, A. D. Meinhaldt, and A. Suna, Appl. Phys. Lett. **47**, 178 (1985).
[43]P. F. Carcia, J. Appl. Phys. **63**, 5066 (1988).
[44]B. N. Engel, C. D. England, R. A. Van Leeuwen, M. H. Wiedmann, and C. M. Falco, Phys. Rev. Lett. **67**, 1910 (1991).
[45]D. Weller, Y. Wu, J. Stohr, M. G. Samant, B. D. Hermsmeier, and C. Chappert, Phys. Rev. B **49**, 12888 (1994).
[46]N. Nakajima, T. Koide, T. Shidara, H. Miyauchi, H. Fukutani, A. Fujimori, K. Iio, T. Katayama, M. Nyvlt, and Y. Suzuki, Phys. Rev. Lett. **81**, 5229 (1998).
[47]J. Thiele, C. Boeglin, K. Hricovini, and F. Chevrier, Phys. Rev. B **53**, R11934 (1996).
[48]A. Sinsarp, T. Manago, F. Takano, and H. Akinaga, Jpn. J. Appl. Phys. **46**, L4 (2006).
[49]C. L. Canedy, X. W. Li, and G. Xiao, Phys. Rev. B **62**, 508 (2000).
[50]M. Bjorck, G. Andersson, B. Sanyal, M. Hedlund, and A. Wildes, Phys. Rev. B **79**, 085428 (2009).
[51]I. Galanakis, M. Alouani, and H. Dreyssé, Phys. Rev. B **62**, 6475 (2000).
[52]T. A. Tyson, S. D. Conradson, R. F. C. Farrow, and B. A. Jones, Phys. Rev. B **54**, R3702 (1996).
[53]S. Ruegg, G. Shutz, P. Fisher, R. Wienke, W. B. Zeper, and H. Ebert, J. Appl. Phys. **69**, 5655 (1991).
[54]G. Shutz, S. Stahler, M. Knulle, P. Fisher, S. Parkin, and H. Ebert, J. Appl. Phys. **73**, 6430 (1993).
[55]C. Ederer, M. Komelj, M. Fahnle, and G. Schutz, Phys. Rev. B **66**, 094413 (2002).
[56]M. Suzuki, H. Muraoka, Y. Inaba, H. Miyagawa, N. Kawamura, T. Shimatsu, H. Maruyama, N. Ishimatsu, Y. Isohama, and Y. Sonobe, Phys. Rev. B **72**, 054430 (2005).
[57]A. Lehnert, S. Dennler, P. Blonski, S. Rusponi, M. Etzkorn, G. Moulas, P. Bencok, P. Gambardella, H. Brune, and J. Hafner, Phys. Rev. B **82**, 094409 (2010).
[58]O. Sipr, J. Minar, S. Mankovsky, and H. Ebert, Phys. Rev. B **78**, 144403 (2008).
[59]M. Ruderman and C. Kittel, Phys. Rev. **96**, 99 (1954).
[60]P. Bruno, Phys. Rev. B **52**, 411 (1995).
[61]J. W. Knepper and F. Y. Yang, Phys. Rev. B **71**, 224403 (2005).
[62]Z. Y. Liu, F. Zhang, N. Li, B. Xu, J. L. He, D. L. Yu, and Y. J. Tian, Phys. Rev. B **77**, 012409 (2008).
[63]Z. Y. Liu, F. Zhang, H. L. Chen, B. Xu, D. L. Yu, J. L. He, and Y. J. Tian, Phys. Rev. B **79**, 024427 (2009).
[64]O. K. Andersen, Phys. Rev. B **12**, 3060 (1975).
[65]D. D. Koelling and G. O. Arbman, J. Phys. F **5**, 2041 (1975).
[66]E. Wimmer, H. Krakauer, M. Weinert, and A. J. Freeman, Phys. Rev. B **24**, 864 (1981).
[67]M. Weinert, E. Wimmer, and A. J. Freeman, Phys. Rev. B **26**, 4571 (1982).
[68]S. Blügel and G. Bihlmayer, in *Computational Nanoscience: Do It Yourself!*, edited by J. Grotendorst, S. Blügel, and D. Marx, NIC Series Vol. 31 (John von Neumann Institute for Computing Press, Jülich, 2006), p. 85.
[69]http://www.fleur.de
[70]J. P. Perdew, K. Burke, and M. Ernzerhof, Phys. Rev. Lett. **77**, 3865 (1996).
[71]G. H. O. Daalderop, P. J. Kelly, and M. F. H. Schuurmans, Phys. Rev. B **44**, 12054 (1991).
[72]P. Ravindran, A. Kjekshus, H. Fjellväg, P. James, L. Nordström, B. Johansson, and O. Eriksson, Phys. Rev. B **63**, 144409 (2001).
[73]W. A. Harrison, *Electronic Structure and Properties of Solids* (Freeman, San Francisco, 1980), Chap. 20.
[74]J. Stöhr, J. Magn. Magn. Mater. **200**, 470 (1999).
[75]P. Bruno, Phys. Rev. B **39**, 865 (1989).
[76]G. van der Laan, J. Phys.: Condens. Matter **10**, 3239 (1998).
[77]G. Schmidt, J. Phys. D **38**, R107 (2005).
[78]A. T. Hanbicki, B. T. Jonker, G. Itskos, G. Kioseoglou, and A. Petrou, Appl. Phys. Lett. **80**, 1240 (2002).
[79]H. X. Yang, M. Chshiev, B. Dieny, J. H. Lee, A. Manchon, and K. H. Shin, Phys. Rev. B **84**, 054401 (2011).
[80]P. LeClair, H. J. M. Swagten, J. T. Kohlhepp, R. J. M. van de Veerdonk, and W. J. M. de Jonge, Phys. Rev. Lett. **84**, 2933 (2000).
[81]P. LeClair, J. T. Kohlhepp, H. J. M. Swagten, and W. J. M. de Jonge, Phys. Rev. Lett. **86**, 1066 (2001).
[82]W. E. Bailey *et al.*, Phys. Rev. B **86**, 144403 (2012).